THE JOURNAL OF PHYSICAL CHEMISTRY C

Article

pubs.acs.org/JPCC

Fast One-Step Synthesis of Biocompatible ZnO/Au Nanocomposites with Hollow Doughnut-Like and Other Controlled Morphologies

Jun Geng,[†,‡] Guang-Hui Song,[†] Xiang-Dong Jia,[†] Fang-Fang Cheng,[†] and Jun-Jie Zhu*[,†]

[†]State Key Laboratory of Analytical Chemistry for Life Science, School of Chemistry and Chemical Engineering, Nanjing University, Nanjing 210093, P. R. China

[‡]Department of Chemistry, Jiangsu Institute of Education, Nanjing 210013, P. R. China

ABSTRACT: Hollow doughnut-like ZnO/Au nanocomposties have been synthesized through a fast one-step microwave-assisted hydrothermal route. The formation mechanism of the product is closely connected with the coordination and selective adsorption effect of trisodium citrate (TSC). Other different structures, such as ZnO nanorods/Au nanoparticles, ZnO nanodisks/Au nanoparticles, and ZnO nanospheres/Au nanoparticles have also been obtained in control experiments. The UV−vis and photoluminescence properties of the as-prepared hollow structures with different Au concentrations showed tunable UV and visible emission intensity. The hollow ZnO/Au nanocomposites are photostable with a strong resonance Raman signal. The colorimetric 3-(4,5-dimethylthiazol-2-yl)-2,5-diphenyl tetrazolium bromide (MTT) assays showed that ZnO/Au nanomaterials have low biological cytotoxicity on human colon cancer cells (LOVO cells) at the concentration of 50 μg/mL. The as-prepared ZnO/Au nanocomposites with good biocompatibility may have potential applications in biomedicine and biosensors.

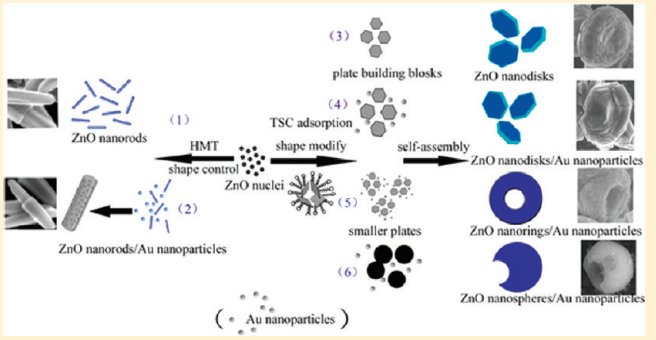

1. INTRODUCTION

The optical, electronic, and magnetic properties of semiconductor and metal nanoparticles have been investigated intensively, and their functionality has been improved by forming hybrid nanocrystals.[1−3] Particularly, the presence of metal nanoparticles on the surface of semiconductor nanostructures was expected to change the optical and electronic properties due to the couplings of metal and semiconductor.[4,5] The noble metal nanoparticles possess many unique properties such as easy reduction, high chemical stability, and bioaffinity;[6−8] in addition, they can enhance the activity of photocatalyst due to good charge storage capability.[9] As the noble metal nanoparticles are combined with the semiconductor nanocrystals, the as-formed hybrid nanocrystals exhibit photoluminescence (PL) properties superior to that of pure semiconductor nanocrystals.[10] Coupling of an oxide semiconductor and noble metal also allows tailoring of surface plasmon resonance (SPR) by electron transfer for plasmon-based chemical and biological sensors.[11,12]

As an important II−VI semiconductor with a wide bandgap (3.37 eV) and a large exciton binding energy (60 meV), ZnO has received much attention over the past decade due to its unique optical, acoustic, and electronic properties.[13,14] Meanwhile, they are more environmentally friendly than those Cd-containing semiconductor nanocrystals.[15] Meanwhile, Au nanoparticles have attracted considerable attention because of their remarkable catalytic and optical properties and numerous potential applications in surface-enhanced Raman scattering and chemical and biological sensing.[16−18] Au is explored to combine ZnO QDs to obtain biocompatible and water-soluble material. The hybrid nanostructures containing Au and ZnO are the attractive nanocomposites due to their novel or enhanced performances, such as very promising nonlinear optical properties,[19] efficient fluorescence resonance energy transfer properties,[20] and enhanced sensitivity in detecting CO gas.[21] The electric field enhancement in biocompatible ZnO/Au nanocomposites can generate strong resonance Raman signals that can be used for ultrasensitive DNA[22] and protein[23] detection.

Although there are some reports concerning the synthesis of ZnO/Au nanocomposites, the morphology of final products is only confined to ZnO nanoparticles/Au nanoparticles[11,22] and ZnO nanorods/Au nanoparticles.[24−26] No other morphology has been reported. Besides, it was found to be difficult to control the size and morphology of the hybrid nanocrystals.[11,27,28] In the present work, a ZnO/Au nanocomposite with special hollow doughnut-like structure was fabricated via a fast one-step microwave-assisted hydrothermal method. The reaction conditions were investigated to find the key factor in the formation of this hollow structure. Other structures, such as ZnO nanorods/Au nanoparticles, hexagonal ZnO nanodisks/Au nanoparticles, and ZnO nanospheres/Au nanoparticles

Received: December 15, 2011
Revised: January 20, 2012

   dx.doi.org/10.1021/jp212092h | J. Phys. Chem. C XXXX, XXX, XXX−XXX

could also be obtained by controlling experimental conditions. The UV−vis absorption and photoluminescence spectra were measured to show the interaction of the ZnO framework and Au nanoparticles. Strong resonance Raman spectroscopic signals under the excitation of an ultraviolet laser could be obtained for the as-prepared ZnO/Au nanocomposites. The cytotoxicity of the nanocomposites has been evaluated. To our best knowledge, controlled synthesis of hollow ZnO/Au nanocomposites with enhanced resonance Raman signal and tunable visible emission intensity has not been reported so far.

2. EXPERIMENTAL SECTION

2.1. Materials. All the reagents used were of analytical purity and were used without further purification. $Zn(NO_3)_2{\cdot}6H_2O$ and hexamethylenetetramine (HMT) were purchased from Beijing Chemical Reagents Company Limited of China. Chloroauric acid ($HAuCl_4$) and trisodium citrate (TSC) were obtained from Shanghai Reagent Company of China. 3-(4,5-Dimethylthiazol-2-yl)-2,5-diphenyl tetrazolium bromide (MTT) was purchased from AMRESCO, and dimethylsulfoxide (DMSO) was obtained from Sinopharm Chemical Reagent Company Limited of China.

2.2. Apparatus. A microwave synthetic system (CEM Discover, USA) was used for the preparation of ZnO/Au nanocrystals, which was equipped with controllable temperature and pressure units. The system can operate at 2450 MHz frequency and work at 0−300 W power. The reaction temperature, pressure, and time can be programmed. The syntheses of nanocrystals were preformed in a cylindrical digestion vessel that was a high-strength vessel consisting of a special kind of glass. The volume of the vessel used in the reaction was 80 mL.

The X-ray powder diffraction (XRD) analysis was performed on a Japan Shimadzu XRD-6000 powder X-ray diffractometer at a scanning rate of 4°/min in the 2θ range from 10° to 80°, with graphite-monochromatized Cu Kα radiation (λ = 0.15418 nm). The scanning electron micrographs (SEM) were taken on an LEO-1530VP field-emission scanning electron microscope. Transmission electron microscopy (TEM) was carried out on a HITACHI H-7650 transmission electron microscope, using an accelerating voltage of 200 kV. High-resolution transmission electron micrographs (HRTEM), selected area electron diffraction (SAED) patterns, and energy dispersive X-ray (EDX) analysis were obtained by employing a JEOL-2010 high-resolution transmission electron microscope with an accelerating voltage of 200 kV. UV−vis absorption spectra were obtained using a Shimadzu UV-3600 spectrophotometer. Photoluminescence spectra (PL) were measured on a Shimadzu RF-5301PC fluorescence spectrometer at room temperature. Resonanace Raman scattering spectra were taken on a Labram HR800 spectrophotometer (Jobin Yvon, France) with the excitation wavelength of 325.0 nm.

2.3. Synthesis. Typically, $Zn(NO_3)_2{\cdot}6H_2O$ (0.0025 mol) was dissolved in 25 mL of H_2O, and then HMT (0.0025 mol) was introduced with stirring to form a clear solution A. An amount of 1 mL of 1% $HAuCl_4$ was introduced to the solution containing 15 mL of 5 mmol·L^{-1} TSC to make solution B. The mixture of solution A and B was transferred to an 80 mL cylindrical digestion vessel under agitation. The reaction was maintained at 100 °C and 175 psi for 30 min under microwave irradiation (260 W). A purple precipitate was centrifuged, washed with distilled water and absolute ethanol in sequence, and finally dried in air. The final products were collected for characterization.

2.4. Cell Cytotoxicity Measurement. Human colon cancer cells (LOVO cells) were plated in a 96-well plate at 1 × 10^4 cells/well. After 24 h incubation, the medium was replaced with 100 μL of fresh medium containing the ZnO/Au nanocomposites at different concentrations (50, 25, 10, 5, 1, and 0 μg·mL^{-1}). Cells were kept at 37 °C for 24 and 48 h. Then the medium was removed, and 100 μL of fresh serum-free medium containing 20 μL of colorimetric 3-(4,5-dimethylthiazol-2-yl)-2,5-diphenyl tetrazolium bromide (MTT, 5 mg/mL, in PBS) was added into each well. After 4 h of incubation, MTT was converted into an insoluble purple formazan dye by mitochondrial dehydrogenases of living cells. The media were removed, and cells were lysed with dimethyl sulfoxide (DMSO). Absorbance was measured at 490 nm using a microplate reader (Bio-Rad 680, USA) to assess the relative viability of the cells. The following formula was used to calculate the inhibition of cell growth

$$\text{Cell viability (\%)} = (\text{mean absorbance value of the treatment group}/\text{mean absorbance value of control}) \times 100\%$$

3. RESULTS AND DISCUSSION

3.1. Characterization of the Final Products. Figure 1 shows the XRD pattern of the as-prepared product. A

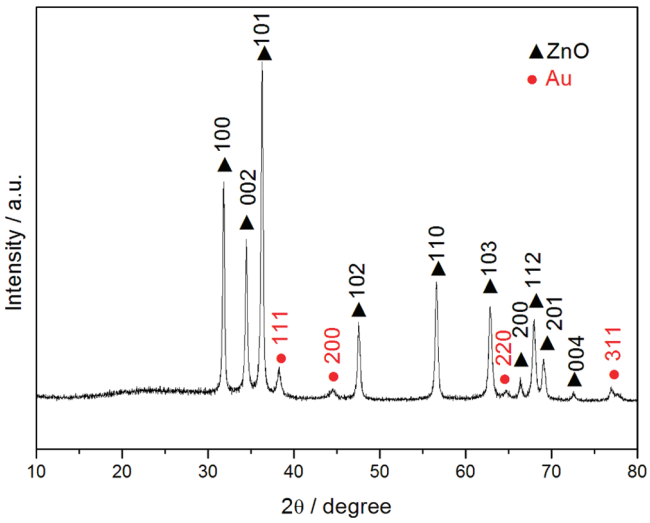

Figure 1. XRD pattern of the as-prepared hollow ZnO/Au nanocomposites.

hexagonal phase ZnO structure (space group $P6_3mc$) is found coexistent with cubic phase Au (space group Fm_3m) in the XRD pattern of the composite structures. All of the diffraction peaks in the XRD pattern are well assigned to ZnO and Au as reported in JCPDS card No. 36-1451 and 04-0784, respectively.

The morphologies of ZnO/Au nanocomposites were observed by SEM and TEM images. Figure 2a−c shows the typical SEM images of the as-prepared hollow ZnO/Au nanocrystals. It is clearly demonstrated that the crystals have a special hollow doughnut-like structure with an outer diameter of 800 nm and an inner diameter of about 250 nm. The shell of the hollow structure seems to be composed of flake-like

dx.doi.org/10.1021/jp212092h | J. Phys. Chem. C XXXX, XXX, XXX−XXX

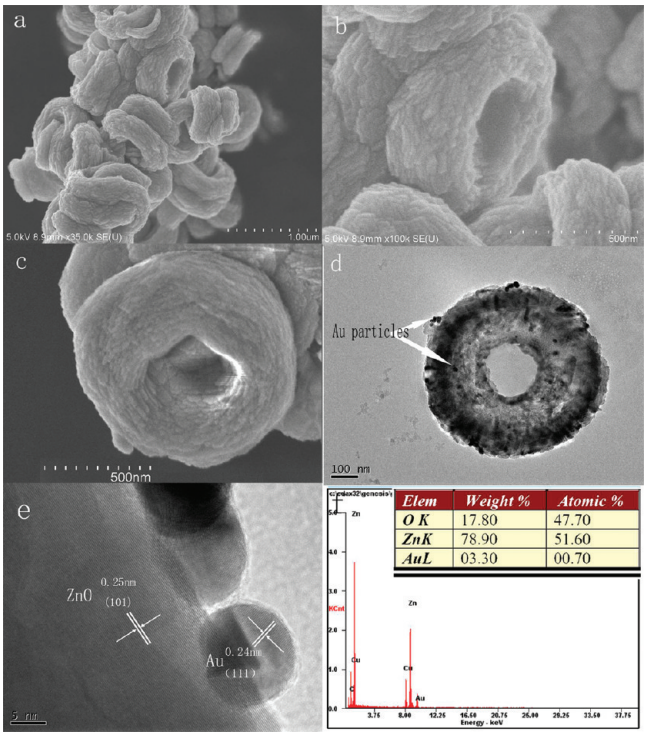

Figure 2. (a) Low-magnification and (b,c) high-magnification SEM images, (d) TEM image, (e) HRTEM image, and (f) EDX spectrum of the as-prepared hollow doughnut-like ZnO/Au nanocomposites with a ratio of Au at 1%.

building blocks. The morphology and microstructure of the as-synthesized ZnO/Au hollow crystals were further studied by TEM and HRTEM. Figure 2d shows that the as-prepared ZnO/Au sample appears as hollow nanodoughnuts with diameter of ca. 800 nm. A strong contrast difference between the edges (dark) and centers (bright) indicates hollow interiors with a wall thickness of about 250−300 nm. Small dark Au nanoparticles with size of about 10 nm could be detected (Figure 2d). In our synthetic route, $HAuCl_4$ was reduced at the same time when ZnO was formed. Therefore, Au nanoparticles were located randomly in the framework or on the surface of ZnO. The HRTEM image obtained on the surface of a nanoring (Figure 2e) indicates clear interplanar spacings of 0.25 nm, corresponding to the (101) crystal faces of ZnO. The HRTEM image recorded on the small dark nanoparticles shows interplanar spacings of 0.24 nm, which could be indexed to the (111) crystal faces of cubic phase Au. To further confirm the composition of the product, EDX spectra were recorded. The EDX spectrum acquired from one doughnut-like structure (Figure 2f) reveals the presence of Zn, O, and Au with an atomic percentage of 51.60%, 47.70%, and 00.70%, which is with an approximate atomic ratio of 1.000:0.924:0.014. This spectrum indicates that the as-prepared product is ZnO/Au nanocomposites with a ratio of Au at about 1%.

3.2. Possible Formation Mechanism. Control experiments were conducted to investigate the possible formation mechanism of the special hollow doughnut-like nanostructure. The relationship between different reaction systems and final products was summarized in Table 1 and Figure 3.

When reactants only concluded Zn^{2+} and HMT, pure ZnO lipstick-like nanorods with length of about 600 nm and diameter of about 100 nm were obtained, as shown in Figure 4a and b. SAED measurement showed that these nanorods grew preferentially along the *c*-axis ([001] direction). In this case, HMT is a nontoxic, water-soluble, nonionic cyclic tertiary amine, which can be reversibly converted into ammonia (NH_3) and formaldehyde (HCHO) through heat treatment (eq 1).[29] In the presence of ammonia, the $[Zn(NH_3)_4]^{2+}$ complex can be formed consequently (eq 2). After that, $[Zn(NH_3)_4]^{2+}$ transforms to zinc oxide during the crystallization.[30]

Table 1. Compositions and Morphologies of Products Prepared in Different Reaction Systems

systems	reactants	compositions	morphologies
(1)	Zn^{2+} + HMT	ZnO	ZnO nanorods
(2)	Zn^{2+} + HMT + $HAuCl_4$	ZnO/Au	ZnO nanorods/Au nanoparticles
(3)	Zn^{2+} + HMT + TSC	ZnO	ZnO nanodisks
(4)	Zn^{2+} + HMT + $HAuCl_4$+ 3 mM TSC	ZnO/Au	ZnO nanodisks/Au nanoparticles
(5)	Zn^{2+} + HMT + $HAuCl_4$ + 5 mM TSC	ZnO/Au	ZnO nanorings/Au nanoparticles (hollow doughnut-like nanostructure)
(6)	Zn^{2+}+HMT +$HAuCl_4$+10 mM TSC	ZnO/Au	ZnO nanospheres/Au nanoparticles

$$(CH_2)_6N_4 + 6H_2O \rightarrow 4NH_3 + 6HCHO \quad (1)$$

$$Zn^{2+} + 4NH_3 + 4H_2O \rightarrow Zn(NH_3)_4{}^{2+} + 4H_2O \rightarrow ZnO + 2OH^- + 4NH_4{}^+ + H_2O \quad (2)$$

Additionally, HMT can kinetically control species in solution by coordinating to Zn^{2+} and keeping the free zinc ion with low concentration. HMT can also coordinate to the ZnO crystal, hindering the growth of certain surfaces. With additional systematic studies, one or all of these mechanisms may be found to be responsible for the HMT shape control. Here, HMT acts as a pH buffer by slowly decomposing to provide a gradual and controlled supply of ammonia, which can form ammonium hydroxide as well as complex zinc(II) to form $[Zn(NH_3)_4]^{2+}$.[31,32] Because dehydration of the zinc hydroxide intermediates controls the growth of ZnO, the slow release of hydroxide may have a profound effect on the kinetics of the reaction. A similar shape-controlled effect of HMT for ZnO nanorods has been reported.[33,34]

While 1 mL of 1% $HAuCl_4$ was added in the above reaction system of Zn^{2+} and HMT, ZnO nanorod/Au nanoparticle composites were synthesized as shown in Figure 4c and d. This result showed that $HAuCl_4$ could be reduced by HMT, and the product remained the rodlike morphology because of the shape-control effect of HMT. Thus, ZnO/Au composites can be obtained in a one-pot process utilizing the ammonia and formaldehyde released by HMT during heat treatment.

In another control experiment, 15 mL of 3 mM TSC was added into the reaction system with Zn^{2+} and HMT but without $HAuCl_4$, and pure ZnO hexagonal nanodisks with diameter of 700 nm and thickness of about 200 nm were prepared (Figure 4e and f). SAED result (inset of Figure 4f) revealed that the nanodisks were perpendicular to the *c* axis. The transformation from nanorods to nanodisks indicated that TSC could adjust the morphology, and its effects on shape control surpassed HMT. As we known, ZnO normally has a

dx.doi.org/10.1021/jp212092h | J. Phys. Chem. C XXXX, XXX, XXX−XXX

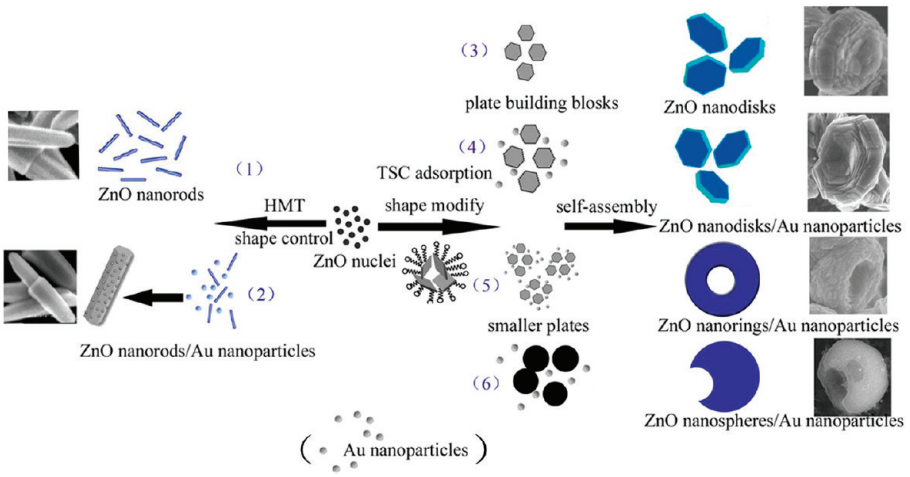

Figure 3. Schematic illustration of the formation of ZnO and ZnO/Au nanostructures.

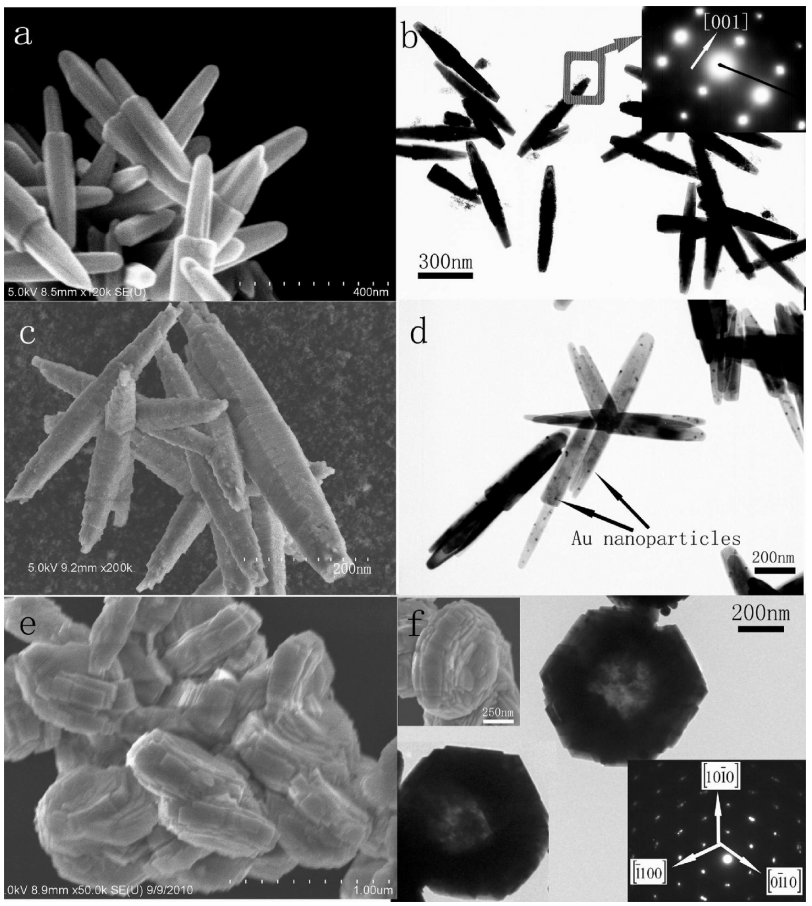

Figure 4. SEM and TEM images of products obtained in different reaction systems: (a, b) ZnO nanorods obtained in the reaction system of Zn^{2+} and HMT, (c, d) ZnO nanorods/Au nanoparticles obtained in the reaction system of Zn^{2+}, HMT, and $HAuCl_4$, and (e, f) ZnO nanodisks obtained in the reaction system of Zn^{2+}, HMT, and TSC. The insets of b and f are the SAED patterns of each product, respectively.

rodlike morphology. The growth of oriented nanodisks is unusual and is directly related to the function of organic acid (citrate), which inhibits the longitudinal growth of rods but promotes the growth of plates. The citrate anion is an important biological ligand which can coordinate with metal ions such as Ag^+, Co^{2+}, Cu^{2+}, Fe^{3+}, Fe^{2+}, Zn^{2+}, and Ni^{2+} to form strong complexes.[35] Besides, it is also a shape modifier.[36] Citrate anions have been known to act as a capping agent of the (0001) surface of the ZnO crystal by adsorbing on the positive polar face of the (0001) surface.[36,37] When citrate anions are adsorbed on the (0001) surface, these citrate anions prevent the contact between $Zn(OH)_4^{2-}$ and the (0001) ZnO crystal surface. As the growth along the [0001] direction is suppressed by citrate anions, ZnO crystal growth will mainly proceed along the six symmetric directions to form hexagonal disks.

In the reaction system containing Zn^{2+}, HMT, $HAuCl_4$, and TSC (15 mL, 5 mM), ZnO nanorings/Au nanoparticles were prepared (Figure 2). Small flake-like building blocks could be

dx.doi.org/10.1021/jp212092h | J. Phys. Chem. C XXXX, XXX, XXX–XXX

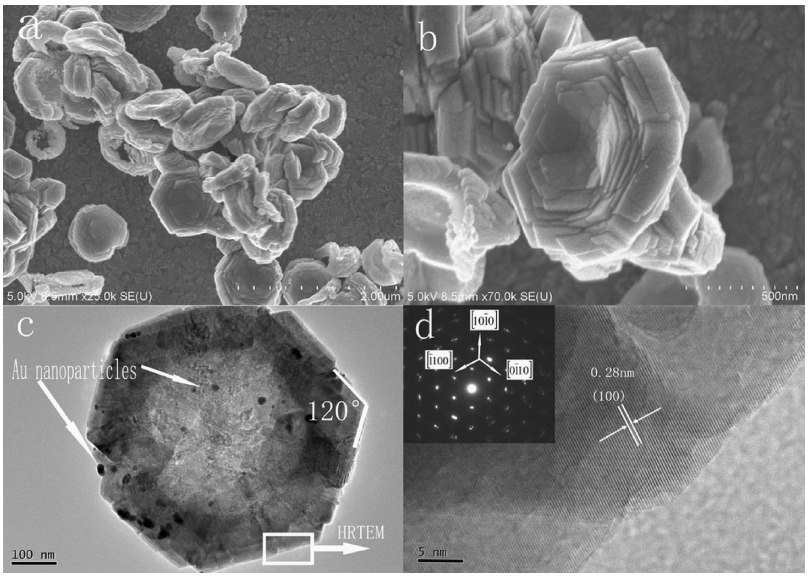

Figure 5. (a) Low-magnification and (b) high-magnification SEM images, (c) TEM image, and (d) HRTEM image of the ZnO nanodisk/Au nanoparticle composites. The inset of d is the SAED pattern of the product.

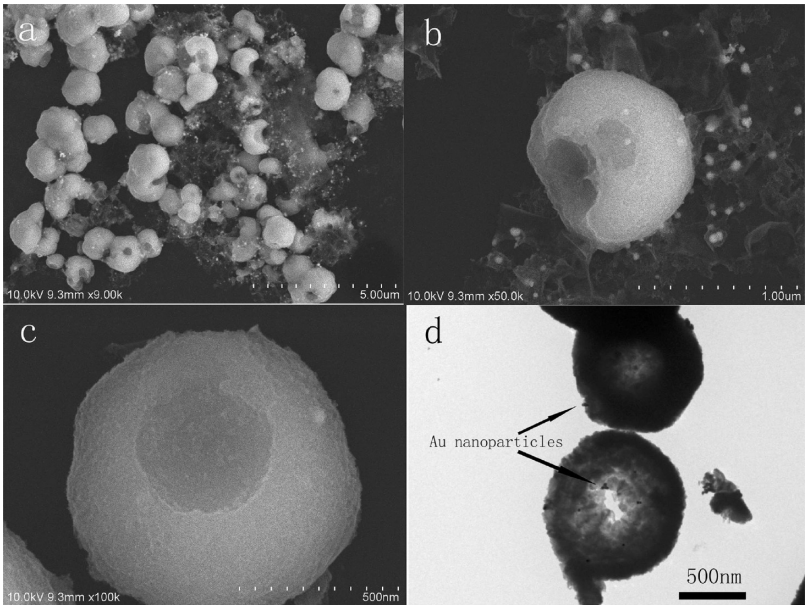

Figure 6. (a) Low-magnification SEM image, (b, c) typical high-magnification SEM images from different angles, and (d) TEM image of the hollow and semihollow spherical ZnO/Au nanocomposites obtained with 10 mM TSC.

detected in the nanostructure. In the growth of ZnO/Au hollow doughnut-like architectures, citrate anions play at least three roles. First, TSC could reduce chloroauric acid to Au nanoparticles. Second, citrate anions coordinate with Zn^{2+} to form citrate−zinc complexes, which prevent the high free zinc ion concentration.[38,39] The formation of citrate−zinc complexes also decreases the generation rate of ZnO nanoparticles in solution. The relatively slow generation rate of ZnO nanoparticles is favorable for the subsequent growth of nanoplates along the determinate direction and the self-assembly to hollow nanorings. Finally, the citrate anion can also serve as a shape modifier which selectively binds to some crystal planes and restricts their growth, whose effect was also applied in the synthesis of ZnO 3D architectures.[36,38] The malate anion, which has a similar molecular structure, plays the same role in the fabrication of ZnO hexagonal architectures.[40] The interaction between citrate anions and nanoparticles would also facilitate crystals to grow along the determinate direction. Besides, there is an interaction between citrate anions binding to the nanoparticles, such as van der Waals forces and intermolecular hydrogen bonds. The interaction would induce the assembly of nanoparticles forming ZnO nanorings and landing Au nanoparticles on the skeleton of ZnO, which further resulted in the formation of ZnO/Au doughnut-like architectures.

In this synthesis, microwave irradiation was fast and highly efficient for transferring energy into the reaction system, and the temperature increased uniformly throughout the reactants.[41] High temperature (100 °C) to the advantage of reducing Au on the ZnO nanocrystals could be easily obtained in 5 min, and a fast and homogeneous nucleation process could be achieved, which improves the crystallinity of the ZnO/Au

dx.doi.org/10.1021/jp212092h | J. Phys. Chem. C XXXX, XXX, XXX−XXX

nanocrystals. In the procedure, the time required to attain good crystallinity and uniform size of ZnO/Au nanocrystals was within half an hour. We have tried control experiments with a shortened reaction time of 10 min, and the same ZnO/Au doughnut-like nanostructure could also be obtained.

3.3. Effect of TSC Concentrations. In the reaction system containing Zn^{2+}, HMT, $HAuCl_4$, and TSC, ZnO nanorings/Au nanoparticles, ZnO nanodisks/Au nanoparticles, or ZnO nanospheres/Au nanoparticles could be prepared according to the concentration of TSC.

When the concentration of TSC was 3 mM, the ZnO nanodisk/Au nanoparticle composite was obtained. The typical SEM image showed that the hexgonal dished nanodisks with diameter of about 600 nm were composed of many hexgonal sheetlike building blocks (Figure 5a and b). TEM image showed that small Au nanoparticles were attached on the hexagonal disks. The angle between two adjacent edges of one disk was measured to be 120°. The SAED pattern recorded on the edge of the structures shows that the ZnO framework is of single-crystal nature with hexagonal phase (inset of Figure 5d). The HRTEM image recorded on the edge of nanodisks shows clear interplanar spacings of 0.28 nm, which can be indexed to the (100) crystal faces of hexagonal phase ZnO. Combined with the SAED measurement, we could draw the conclusion that the nanodisks were perpendicular to the *c* axis.

After increasing TSC concentration to 5 mM, the ZnO nanoring/Au nanoparticle composite was fabricated, as shown in Figure 2. By careful observation, it is found that the nanorings were composed of sheet-like crystals growing layer by layer. The size of these sheet-like building blocks was smaller than that of building blocks in nanodisks prepared with 3 mM TSC. The increase of TSC concentration might cause more citrate−zinc complexes to form and more citrate anions to selectively bind to crystal planes, which therefore restricted their crystal growth and resulted in smaller plates. The increase of TSC also had an effect on the transformation from nanodisks to hollow nanorings. We supposed that the organic acid citrate with suitable concentration might be responsible for the formation of nanorings. However, the exact function of this TSC concentration is not very clear and still under investigation. We think that the synergistic action of TSC, HMT, and Zn^{2+} might be responsible for the formation of hollow nanorings.

Further increasing TSC concentration to 10 mM resulted in hollow and semihollow spherical ZnO/Au nanocomposites, as shown in Figure 6. Some free small Au nanoparticles could also be seen. The disk-like building blocks could not be detected in these spheres, which was different from the above hollow nanorings. The excess amount of TSC might cause extra adsorption and restriction to nanoparticles growth, which resulted in the disappearance of hexagonal disk-like building blocks. More TSC also caused faster reduction of $HAuCl_4$, and therefore more Au nanoparticles did not land on the framework of ZnO but existed as free Au nanoparticles.

3.4. Optical Properties Measurement. ZnO is a wide-band-gap semiconductor (E_g = 3.37 eV) with a large exciton binding energy (60 meV). Optical studies were performed to evaluate the potentially optical qualities of the doughnut-shaped ZnO/Au nanocomposites.

Figure 7 showed the UV−vis absorption spectra of pure ZnO nanorods and ZnO nanoring/Au nanoparticle composites with different Au concentrations. The absorption peaked at 370 nm exhibits a well-defined exciton band of ZnO nanorods (Figure 7a). The calculated band gap is 3.35 eV under current measured conditions, which is in accordance with the bulk values. No quantum confinement effects were observed because of the relatively large size.

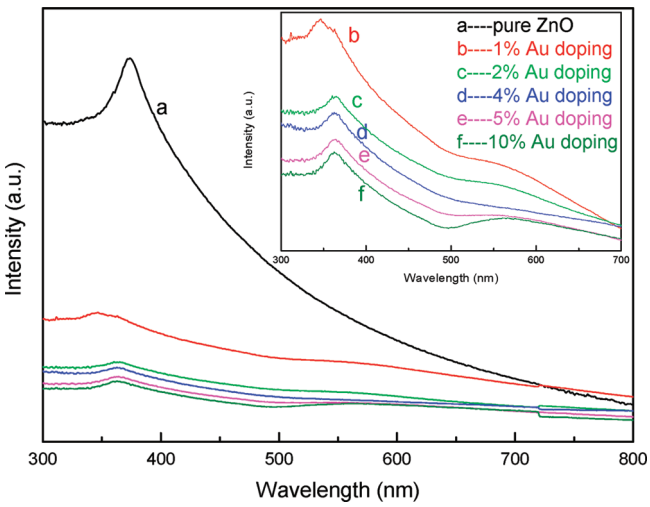

Figure 7. Absorption spectra of (a) pure ZnO and ZnO/Au nanocomposites with a ratio of Au at (b) 1%, (c) 2%, (d) 4%, (e) 5%, and (f) 10%. The inset shows the amplificatory absorption spectra of the ZnO/Au nanocomposites.

The exciton band of ZnO/Au nanocomposites showed a blue-shift to around 360 nm, which may result from the small nanodisk building blocks in the nanocomposites as discussed above. In the inset of Figure 7, it is clear that the plasmon absorption band centered at 550 nm of Au appears with the formation of ZnO/Au nanocomposites. This peak has a red-shift from 540 to 560 nm with the increased amount of Au on the surface of ZnO from 1 to 10%. It can be attributed to the electron transfer between Au and ZnO, which provides support to the formation of the ZnO/Au nanocomposite.[24]

The optical properties of ZnO/Au nanocrystals were further manifested by the room-temperature photoluminescence (PL) spectra under photon excitation of 325 nm. It can be observed that two emission bands appeared in the PL spectra of pure ZnO (Figure 8a). The emission band centered at 363 nm could be attributed to the transition between the band edges, and the band centered at 525 nm in the yellow region could be attributed to the intrinsic defects of oxygen vacancies related emission.[42] As shown in Figure 8b−f, ZnO/Au hybrid nanostructures with different Au concentrations all exhibit stronger UV emission around 360 nm and weaker visible emission at about 500 nm than those of pure ZnO. For ZnO/Au hybrid nanocrystals, upon increasing the amount of Au, the UV emission intensity is enhanced, and the visible emission is suppressed gradually.

There are two possible reasons for the enhancement of UV emission intensity and the decrease of visible emission intensity in the ZnO/Au system:[43,44] (i) the adsorption of visible light by Au can create exciton−surface plasmon coupling, which favors the electron transfer from Au to ZnO, resulting in the enhancement of UV emission intensity, and (ii) the number of single ionized oxygen vacancies (Vo^+) has been decreased/quenched by capturing electrons when more electrons transferred from Au to ZnO. The surface defects of ZnO become fewer and fewer by increasing the amount of Au, and thus the visible emission becomes weaker and weaker in the

dx.doi.org/10.1021/jp212092h | J. Phys. Chem. C XXXX, XXX, XXX−XXX

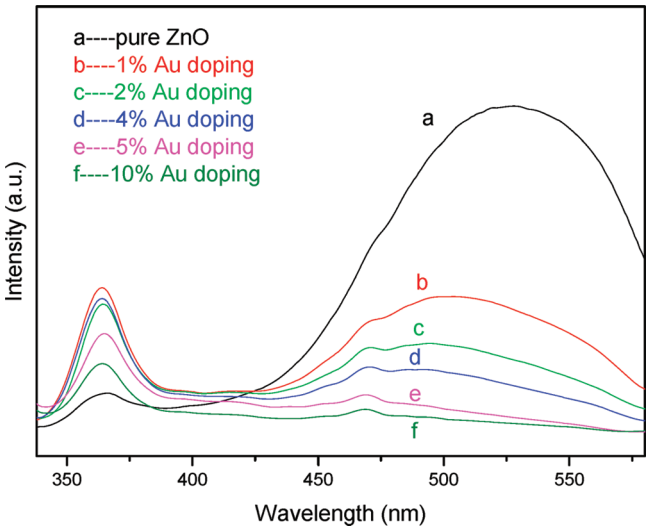

Figure 8. PL spectra of (a) the pure ZnO and ZnO/Au nanocomposites with ratio of Au at (b) 1%, (c) 2%, (d) 4%, (e) 5%, and (f) 10%.

present case, which is similar to ZnO/Ag heterostructures.[43] Even though these two explanations can explain well the bleaching of the visible emission and enhancement of UV emission intensity, the detailed mechanism needs more dedicated work in the future.

3.5. Resonance Raman Scattering Spectra. ZnO quantum dots (QDs) have the characteristic resonance multiple-phonon Raman lines with the excitation wavelength of 325 nm, which can be used as a characteristic fingerprint signal. Upon forming ZnO/Au nanocomposites, the electrons transferred between ZnO and Au nanoparticles can yield the electromagnetic-field enhancement, which further enhances the multiple-phonon Raman scattering of ZnO.[11]

Figure 9 showed the 2D and 3D resonance Raman scattering spectra of pure ZnO and ZnO/Au nanocomposites. In Figure 9a, pure ZnO nanocrystals had a weak resonance Raman signal. The resonance Raman signal of ZnO capped by Au nanoparticles increased as shown in Figure 9b–f. Because the electron transfer between ZnO and Au nanoparticles occurred, the built-in electrical field formed in the interface of ZnO/Au nanocomposites. As a result, ZnO received the stronger local electromagnetic field. The formed local electromagnetic field can interact with optical phonons in ZnO nanocrystals, which enhanced the scattering intensity of active phonons.[11] As shown in Figure 9b–d, with increasing the amount of Au on the surface of ZnO from 1 to 4%, the Raman signal increased. The enhanced intensity indicated more electrons transfer between Au and ZnO and therefore increased the electromagnetic field around ZnO nanocrystals. The electromagnetic field enhancement further enhanced the multiple-phonon Raman scattering of ZnO. However, when the amount of Au on the surface of ZnO was greater than 4%, the Raman intensity decreased (Figure 9e and f). Therefore, the amount of Au was chosen as 4% to obtain an optimal Raman enhancement. The ZnO/Au nanocomposites can serve as a universal biocompatible tag for analyzing various biological macromolecules such as proteins and DNA.

3.6. Cytotoxicity of ZnO/Au Nanocrystals for the LOVO Cell Lines. Colorimetric 3-(4,5-dimethylthiazol-2-yl)-2,5-diphenyl tetrazolium bromide (MTT) assays were performed to estimate the cytotoxicity of the nanocomposites. The MTT assays of the cells showed that ZnO/Au nanomaterials had low cytotoxicity at a concentration of 50 μg/mL on LOVO cell lines (Figure 10) which indicated good biocompatibility and potential applications in biomedicine and biosensor. It is found that the cytotoxicity of ZnO/Au nanocomposites mainly comes from ZnO.[23] Also of note, there was a small increase of cell viability for the ZnO/Au nanocrystals with 24 h incubation, which might arise from the stimulation of cells in the presence of nanoparticles.[45] Other Cd-containing semiconductor nanocrystals, such as CdSe,[15] CdTe,[46] and CdS,[47] are more toxic than ZnO. For example, CdTe QDs of low concentrations (0.75 μM) led to a significant death rate of human erythroleukemia cells (K562 cells) after 24 or 48 h incubation,[46] and these nanocrystals must be coated with some biocompatible shells for biological applications.[15,48]

4. CONCLUSIONS

In summary, hollow doughnut-shaped ZnO/Au nanocomposites have been synthesized via a fast one-step microwave-

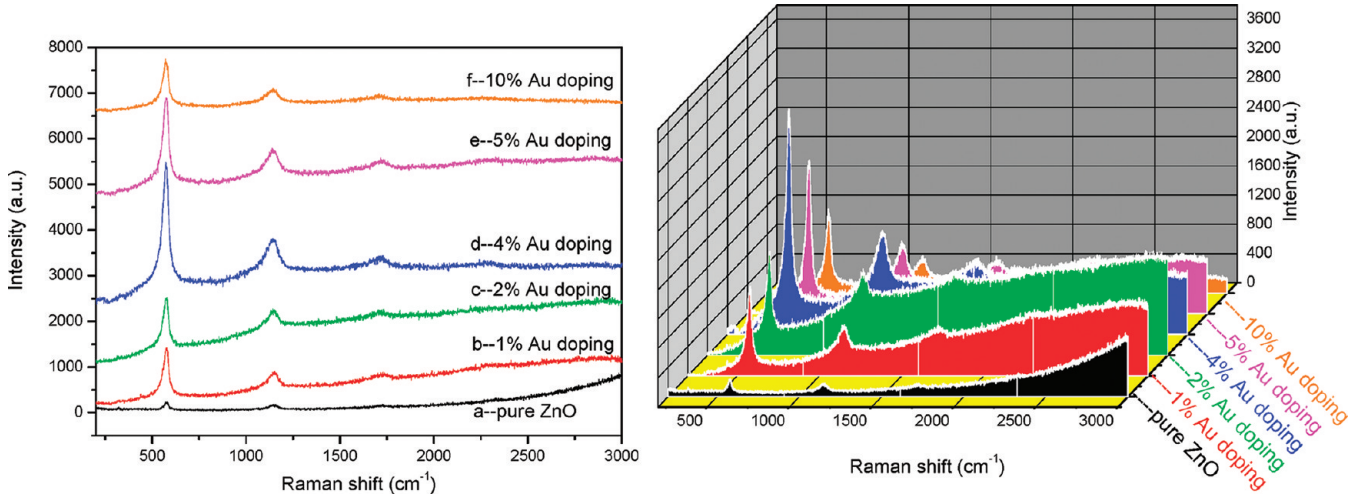

Figure 9. 2D (left) and 3D (right) resonance Raman scattering spectra of (a) pure ZnO and ZnO/Au nanocomposites with ratio of Au at (b) 1, (c) 2, (d) 4, (e) 5, and (f) 10% (λ_{exc} = 325 nm).

dx.doi.org/10.1021/jp212092h | J. Phys. Chem. C XXXX, XXX, XXX–XXX

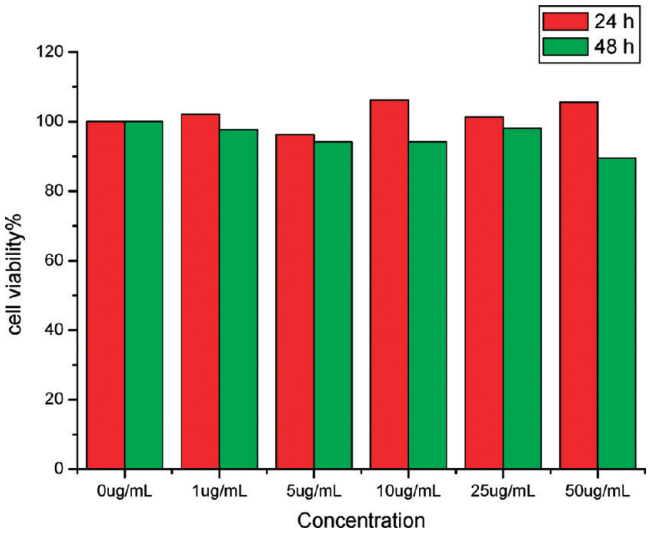

Figure 10. Cell viability of LOVO cells treated with different concentrations of hollow doughnut-shaped ZnO/Au nanocomposites for 24 and 48 h as measured by MTT assays.

assisted hydrothermal route. Citrate salts have been introduced as shape modifiers and proved to be efficient to control the shape of the ZnO/Au nanostructures. Control experiments could also obtain other morphologies which enriched the shape-controlled synthesis of nanocomposites. The PL spectra of ZnO/Au nanocomposites exhibited stronger UV emission and weaker visible emission upon increasing the amount of Au. Compared with pure ZnO, the as-prepared ZnO/Au hybrid crystals showed enhanced multiple-phonon Raman scattering, which could serve as a universal biocompatible tag for analyzing various biological macromolecules such as proteins and DNA. The biological toxicity of the ZnO/Au nanocomposites has been evaluated, and results showed good biocompatibility, which promised a potential application in biomedicine and biosensor.

■ AUTHOR INFORMATION

Corresponding Author

*E-mail: jjzhu@nju.edu.cn. Tel. and Fax: +86-25-83597204.

Notes

The authors declare no competing financial interest.

■ ACKNOWLEDGMENTS

This work is supported by National Natural Science Foundation of China (Grant Nos. 20805022, 21121091) and China Postdoctoral Science Foundation (Grant No. 20100471294). We also thank the support from Doctoral Foundation from Ministry of Education (No. 20100091110023). We thank Ya-Jing Yin from Nanjing Normal University for her kind help in TEM and resonance Raman scattering measurements.

■ REFERENCES

(1) Kim, H.; Achermann, M.; Balet, L. P.; Hollingsworth, J. A.; Klimov, V. I. *J. Am. Chem. Soc.* **2005**, *127*, 544.
(2) Lee, J.; Govorov, A. O.; Dulka, J.; Kotov, N. A. *Nano Lett.* **2004**, *4*, 2323.
(3) Jian, D. L.; Gao, Q. M. *Chem. Eng. J.* **2006**, *121*, 9.
(4) Zhang, W.; Govorov, A. O.; Bryant, G. W. *Phys. Rev. Lett.* **2006**, *97*, 146804.
(5) Lee, J.; Kotov, N. A.; Slocik, J. M.; Naik, R. R. *Nano Lett.* **2006**, *6*, 984.
(6) Daniel, M. C.; Astruc, D. *Chem. Rev.* **2004**, *104*, 293.
(7) Cao, Y. W.; Jin, R. C.; Mirkin, C. A. *J. Am. Chem. Soc.* **2001**, *123*, 7961.
(8) Gill, R.; Polsky, R.; Willner, I. *Small* **2006**, *2*, 1037.
(9) Chan, S. C.; Barteau, M. A. *Langmuir* **2005**, *21*, 5588.
(10) Lin, H. Y.; Chen, Y. F.; Wu, J. G.; Wang, D. I.; Chen, C. C. *Appl. Phys. Lett.* **2006**, *88*, 161911.
(11) Wang, X.; Kong, X.; Yu, Y.; Zhang, H. *J. Phys. Chem. C* **2007**, *111*, 3836.
(12) Ma, G. H.; He, J.; Rajiv, K.; Tang, S. H.; Yang, Y.; Nogami, M. *Appl. Phys. Lett.* **2004**, *84*, 4684.
(13) Wang, Z. L.; Song, J. *Science* **2006**, *312*, 242.
(14) Tang, H. X.; Yan, M.; Ma, X. Y.; Zhang, H.; Wang, M.; Yang, D. R. *Sens. Actuator B: Chem.* **2006**, *113*, 324.
(15) Derfus, A. M.; Chan, W. C. W.; Bhatia, S. N. *Nano Lett.* **2004**, *4*, 11.
(16) Cao, Y. C.; Jin, R.; Mirkin, C. A. *Science* **2002**, *297*, 1536.
(17) Kneipp, K.; Wang, Y.; Kneipp, H.; Perelman, L. T.; Itzkan, I.; Dasari, R. R.; Feld, M. S. *Phys. Rev. Lett.* **1997**, *78*, 1667.
(18) El-Sayed, I. H.; Huang, X.; El-Sayed, M. A. *Nano Lett.* **2005**, *5*, 829.
(19) Ozga, K.; Kawaharamura, T.; Umar, A. A.; Oyama, M.; Nouneh, K.; Slezak, A.; Fujita, S.; Piasecki, M.; Reshak, A. H.; Kityk, I. V. *Nanotechnology* **2008**, *19*, 185709.
(20) Haldar, K. K.; Sen, T.; Patra, A. *J. Phys. Chem. C* **2008**, *112*, 11650.
(21) Chang, S. J.; Hsueh, T. J.; Chen, I. C.; Huang, B. R. *Nanotechnology* **2008**, *19*, 175502.
(22) Liu, Y.; Zhong, M.; Shan, G.; Li, Y.; Huang, B.; Yang, G. *J. Phys. Chem. B* **2008**, *112*, 6484.
(23) Shan, G.; Wang, S.; Fei, X.; Liu, Y.; Yang, G. *J. Phys. Chem. B* **2009**, *113*, 1468.
(24) Zhang, W. Q.; Lu, Y.; Zhang, T. K.; Xu, W. P.; Zhang, M.; Yu, S. H. *J. Phys. Chem. C* **2008**, *112*, 19872.
(25) Chen, B. D.; Zhang, H.; Du, Ning, Li, D. S.; Ma, X. Y.; Yang, D. *Mater. Res. Bull.* **2009**, *44*, 889.
(26) Wei, Y. Y.; Li, Y.; Liu, X. Q.; Xian, Y. Z.; Shi, G. Y.; Jin, L. T. *Biosens. Bioelectron.* **2010**, *26*, 275.
(27) Sabramanian, V.; Wolf, E. E.; Kamat, P. V. *J. Phys. Chem. B* **2003**, *107*, 7479.
(28) Wood, A.; Giersig, M.; Mulvaney, P. *J. Phys. Chem. B* **2001**, *105*, 8810.
(29) Vayssieres, L.; Keis, K.; Hagfeldt, A.; Lindquist, S. E. *Chem. Mater.* **2001**, *13*, 4395.
(30) Yin, S.; Sato, T. *J. Mater. Chem.* **2005**, *15*, 4584.
(31) Liu, B.; Zeng, H. C. *J. Am. Chem. Soc.* **2003**, *125*, 4430.
(32) Wang, Z.; Qian, X. F.; Yin, J.; Zhu, Z. K. *Langmuir* **2004**, *20*, 3441.
(33) Yang, Y. M.; Lai, H.; Tao, C. Y.; Yang, H. *J. Mater. Sci.: Mater. Electron.* **2010**, *21*, 173.
(34) Zhang, Y. Y.; Mu, J. *J. Colloid Interface Sci.* **2007**, *309*, 478.
(35) Parkinson, J. A.; Sun, H. Z.; Sadler, P. J. *Chem. Commun.* **1998**, *8*, 881.
(36) Tian, Z. R.; Voigh, J. A.; Liu, J.; Mckenzie, B.; Mcdermott, M. J.; Rodriguez, M. A.; Konishi, H.; Xu, H. F. *Nat. Mater.* **2003**, *2*, 821.
(37) Xu, L.; Guo, Y.; Liao, Q.; Zhang, J.; Xu, D. *J. Phys. Chem. B* **2005**, *109*, 13519.
(38) Liang, J. B.; Liu, J. W.; Xie, Q.; Bai, S.; Yu, W. C.; Qian, Y. T. *J. Phys. Chem. B* **2005**, *109*, 9643.
(39) Caswell, K. K.; Bender, C. M.; Murphy, C. J. *Nano Lett.* **2003**, *3*, 667.
(40) Liang, J. B.; Bai, S.; Zhang, Y. S.; Li, M.; Yu, W. C.; Qian, Y. T. *J. Phys. Chem. C* **2007**, *111*, 1113.
(41) Qian, H. F.; Li, X. Q.; Ren, J. C. *J. Phys. Chem. B* **2006**, *110*, 9034.
(42) (a) Yang, P.; Yan, H.; Mao, S.; Russo, R.; Johnson, J.; Saykally, R.; Morris, N.; Pham, He, J. R.; Choi, H. J. *Adv. Funct. Mater.* **2002**, *12*,

319. (b) Wu, J. J.; Liu, S. C. *Adv. Mater.* **2002**, *14*, 215. (c) Li, Y. B.; Bando, Y.; Golberg, D. *Appl. Phys. Lett.* **2004**, *84*, 3603.
(43) (a) Wood, A.; Giersig, M.; Mulvaney, P. *J. Phys. Chem. B* **2001**, *105*, 8810. (b) Subramanian, V.; Wolf, E. E.; Kamat, P. V. *J. Phys. Chem. B* **2003**, *107*, 7479.
(44) (a) Bai, X. D.; Wang, E. G.; Gao, P. X.; Wang, Z. L. *Nano Lett.* **2003**, *3*, 1147. (b) Wang, X. D.; Summers, C. J.; Wang, Z. L. *Appl. Phys. Lett.* **2005**, *86*, 013111.
(45) Thayer, K. A.; Melnick, R.; Burns, K.; Davis, D.; Huff, J. *Environ. Health Perspect.* **2005**, *113*, 1271.
(46) Su, Y. Y.; He, Y.; Lu, H. T.; Sai, L. M.; Li, Q. N.; Li, W. X.; Wang, L. H.; Shen, P. P.; Huang, Q.; Fan, C. H. *Biomaterials* **2009**, *30*, 19.
(47) Li, K. G.; Chen, J. T.; Bai, S. S.; Wen, X.; Song, S. Y.; Yu, Q.; Li, J.; Wang, Y. Q. *Toxicol. in Vitro* **2009**, *23*, 1007.
(48) (a) Lovric, J.; Bazzi, H. S.; Cuie, Y.; Fortin, G. R. A.; Winnik, F. M.; Maysinger, D. *J. Mol. Med.* **2005**, *83*, 377. (b) Sasanka, D.; Alessandra, Q.; Grazia, L. M. *J. Am. Chem. Soc.* **2009**, *131*, 2948.